

Optimization of a lidar receiving system. Spatial filters

A.I. Abramochkin and A.A. Tikhomirov

*Institute of Optical Monitoring,
Siberian Branch of the Russian Academy of Sciences, Tomsk*

Received December 25, 1998

Operation of several types of spatial filters (SF) is analyzed from the viewpoint of unified principles of constructing images of a scattering volume and its transmission through a spatial filter of a lidar. Diaphragms of several shapes and rasters are considered as SF that define the angular field of view of a lidar receiving system. The main characteristics and efficiency criteria for SF are listed. The shape of matching and optimum diaphragms increasing the signal-to-noise ratio is determined. Diaphragms and rasters intended for controlled vignetting of the transmitted radiation flux within a given range are compared. Several types of lidar SF for isolating multiple scattering and other applications are also considered in the paper.

1. Introduction

Earlier, in Ref. 1, we have discussed a comparison among lidar receiving objectives of different types. The spatial filter (SF) is the second element of a receiving system. It effects the radiation flux directed to a lidar photodetector. The term "spatial filter", as applied to lidar technique, refers to an element that forms the field of view of a receiving system in the space of objects (solid angle). Below, by spatial filtration we understand the following: 1) isolation of the backscattered radiation flux (lidar return signal) having finite angular dimensions, against the background of spatially distributed radiation of noise sources; 2) separation of individual parts of the received radiation flux arriving at different angles; 3) linear transformations of the intensity of this radiation with the elements of the receiving system.

Mainly, diaphragms of several shapes are used as the SF.² The diaphragms define the angular field of view of the receiving system. SF defines also the transmission coefficient of the receiving system, which depends on distance²⁻⁹ (i.e., the lidar geometrical factor), and restricts the dynamic range of a lidar return.¹⁰ Besides, SF permits one to analyze the energy structure of the received radiation flux and estimate the contribution of multiple scattering components to it.¹¹⁻¹³ The input end of an optical wave guide transmitting the radiation flux from the receiving objective to the photodetector can also be a part of an SF.^{13,14} The entrance slit of the spectral device is used as SF in Raman lidars.¹⁵ The next type of SF are rasters of various types (optical wedges,¹⁶ mirrors,¹⁸ and vignetting diaphragms of some particular profiles^{2,18}) which guarantee compensation for the inverse square range (z^{-2}) fall off of return signal.

In this paper, we generalize the results on spatial filtration of lidar signals and describe technical solutions used for these purposes.

2. Intention and main characteristics of spatial filters of the lidar receiving systems

SF of a lidar receiving system is intended for several purposes. First, it reduces the influence of background radiation noise on the operation of a photodetector. Second, its dimensions and position in the system define the range boundaries of lidar return reception. Third, the shape and transmission coefficient of a SF define the geometrical factor of the lidar, which is a function of distance $g(z)$, what makes it possible to control the signal received from a given range interval. Fourth, the shape and position of a SF enables one to separate the components of the radiation flux that are caused by multiple scattering and polarization.

The main SF characteristics that define the value of the radiation flux passing through the filter are as follows: 1) the shape and the area of its aperture; 2) the function $f(x, y)$ describing SF transmittance with respect to the axes of the filter's coordinates; 3) displacement in the position of the SF installation with respect to the focal plane of the objective z_0 ; 4) displacement of the SF center and other SF characteristics points with respect to the optical axis of the receiving system; 5) the limiting incidence angle u of a ray entering the SF.

The shape and the area of the SF aperture, together with the focal distance of the objective f_r define the angular field of view of the receiving system. The field is characterized by solid angle Ω which is not a cone in the general case (Fig. 1e). For a SF placed in the focal plane and having the shape of a round aperture with the diameter $2a$, the solid angle is $\Omega = \pi(a/f_r)^2$ where the full plane angle of the field is $\theta_r = 2a/f_r$.

The function $f(x, y)$ has three main forms. For a simple pin hole, $f(x, y) = 1$ over the whole filter area (Fig. 1b). SF for that is used for investigating multiple scattering has a more complicated form of $f(x, y)$, e.g., "meander" (Fig. 1c). For the SF that compensates for z^{-2} dependence of a lidar return, the form of the normalized function $\overline{f(x, y)} = \overline{f(y)}$ is shown in Fig. 1d as a parabola. The shape of a SF, displacement of its geometrical center with respect to the optical axis

of the objective h , and the transmission function $f(x, y)$ are considered below in the SF coordinate system which is related to that of the receiving objective. The restriction imposed on the incidence u of the flux is connected, for instance, with the SF finite thickness and with the number aperture $A = \sin u = (n_f^2 - n_o^2)^{1/2}$ of optical wave guides. Here n_f and n_o are refractive indices of the fiber core and its cladding, respectively.²⁰

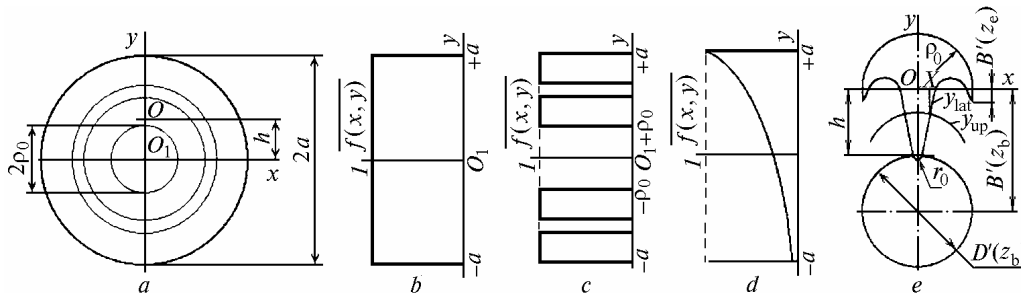


Fig. 1. Spatial filters in the form of diaphragms: round decentered (a) and its normalized transmission function (b); $\overline{f(x, y)}$ of the SF for separating multiple scattering orders (c); $\overline{f(x, y)}$ of the compensating SF (d); the shape of the diaphragm compensating for z^{-2} (e); O is the projection of the optical axis of the objective onto the SF plane.

The term "field stop" which is now used in lidar technology, is not quite correct according to Ref. 21, because the diaphragm is not constantly in the plane of the scattering volume image because the latter permanently moves in the image space behind the objective. So, a round-shaped diaphragm is vignetting within a certain range interval.

3. Imaging of a scattering volume in the approximation of geometrical optics

Analysis of the SF operation has been generalized using the results obtained in Refs. 3–8 devoted to formation of the image of a scattering volume which is

formed by a laser pulse in a medium sounded. Figure 2 presents the optical arrangement of sounding with a biaxial lidar having the separation B_0 and the angle γ between the optical axes of the receiving and transmitting systems whose aperture diameters are D_r and D_0 , respectively. The axis OZ of the cylindrical coordinate system is aligned with the optical axis of the receiving system. The angle $\gamma = (\gamma_{||}^2 + \gamma_{\perp}^2)^{1/2}$, and the angles $\gamma_{||}$ and γ_{\perp} characterize the slopes in the planes YOZ and XOZ (the positive value of $\gamma_{||}$ corresponds to intersection of the projection of the axis O_1O_1 with the OZ axis in the space of objects). Let us consider the diaphragm of diameter $2a$ as a SF. The diaphragm is displaced from the focal plane of the objective by the distance $+z_0$.

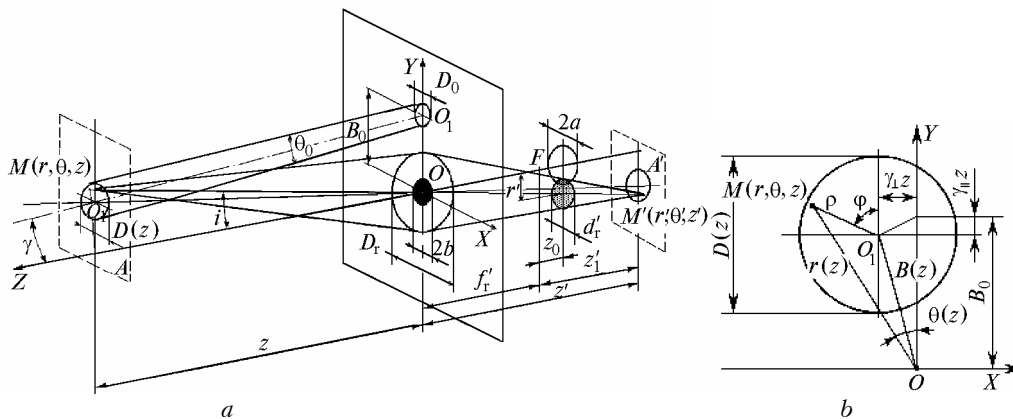


Fig. 2. Construction of the scattering volume image in the receiving system of a lidar: general view (a); section of the scattering volume in the plane A (b).

Within the circle of $D(z) = D_0 + \theta_0 z$ (Fig. 2a) diameter, illumination at the point $M(r, \theta, z)$ is characterized by the expression $E(\rho, \varphi, z) = P_0 T(z) \kappa(\rho, \varphi) / [\pi D^2(z)/4]$, where θ_0 is the divergence angle of the sounding beam; ρ, φ are the polar coordinates in its cross section (Fig. 2b); P_0 is the pulse power; $T(z)$ is the atmospheric transmission; $\kappa(\rho, \varphi)$ is the factor taking into account the distribution of the radiation intensity that satisfies the condition $[4/\pi D^2(z)] \int_0^{D(z)/2} \rho d\rho \int_0^{2\pi} \kappa(\rho, \varphi) d\varphi = 1$. In

the general case, illumination is inhomogeneous over the cross section due to both the mode structure of laser radiation and its turbulent distortions in the atmosphere.

We assume the return signal to be described in the single scattering approximation at the distances much larger than the spatial length of the sounding laser pulse, i.e., $z \gg c \tau/2$. At smaller z , it is necessary to take into account the shape of sounding pulse. Using the expression for reflection coefficient of the scattering volume $\eta(z) = (c\tau/2) \beta_\pi(z)$, where $\beta_\pi(z)$ is the backscattering coefficient, one can define the value of the radiation flux scattered by an infinitesimal surface element $dS = r dr d\theta$ from the neighborhoods of the point $M(r, \theta, z)$ and incident onto the entrance aperture as:

$$dP(r, \theta, z) = \eta(z) P_0 \kappa(\rho, \varphi) T^2(z) A_{\text{eff}} r dr d\theta / [\pi D^2(z) z^2 / 4], \quad (1)$$

where $A_{\text{eff}} = \pi D_r^2/4$ for a lens objective or $A_{\text{eff}} = \pi(D_r^2/4 - b^2)$ for a mirror objective with the secondary mirror of $2b$ diameter. The angle i of the slant incidence of radiation onto the objective arrived from the above mentioned large distances z and bases B_0 is such that $\cos i \cong 1$.

The projection of the point M moves in the plane XOY while z increases, as the angle between the optical axes γ differs from zero. The polar coordinate system of the beam cross section ρ, φ relates to the coordinate system r, θ, z (see Fig. 2) via the transform

$$\begin{cases} \rho^2(z) = r^2(z) + B^2(z) - 2r(z) B(z) \cos\theta(z), \\ \varphi(z) = \arcsin\{[r(z)/\rho(z)] \sin \theta(z)\}, \\ r^2(z) = (r_1 - \gamma_{\parallel} z)^2 + (\gamma_{\perp} z)^2, \\ B^2(z) = (B_0 - \gamma_{\parallel} z)^2 + (\gamma_{\perp} z)^2, \\ \theta(z) = \theta_1 + \arctan[\gamma_{\perp} z / (B_0 - \gamma_{\parallel} z)], \end{cases} \quad (2)$$

where r_1 and θ_1 are the coordinates of the projection of the $M(r, \theta, z)$ point onto the plane of lidar apertures (XOY). For a purely coaxial system $\gamma = 0$, B_0 equals zero, and the formulas (2) reduce to a simpler form.

In the approximation of paraxial optics,²⁰ the image of the point M is at a distance $z'(z) = f_r^2 / (z - f_r)$ behind the focal plane being at the same time

displaced from the optical axis at the distance $r'(z) = r(z) f_r / (z - f_r)$. The rays coming from the point M form a diffuse circle in the diaphragm plane. Its diameter is

$$d'_r = v D_r f_r / z, \quad (3)$$

and center is displaced from the optical axis by the distance $r' = \zeta r(z) f_r / z$, where $v = \zeta - z_0 z / f_r^2$ and $\zeta = 1 + z_0 / f_r$. The coefficient v characterizes the degree of defocusing of the point M image in the diaphragm plane. For a given z_0 , there exists a unique conjugate plane in the space of objects for which the point M is represented also by a point. It is at the distance z_c from the objective, $z_c = f_r (1 + f_r / z_0)$. In all other cases, a converging or diverging cone-shaped beam passes through the diaphragm from the point M . It forms a diffuse circle with the area

$$S'_M(z) = \pi (v f_r D_r / 2z)^2 = (v f_r / z)^2 A_{\text{eff}}. \quad (4)$$

Illumination within the circle, without a regard for edge and diffraction effects, can be considered to be homogeneous and equal to $dE(r', \theta', z') = dP(r, \theta, z) K_t / S'_M(z)$, where K_t is the objective's transmission coefficient. Thus formed illumination is created by light from each point of the cross section $D(z)$. The total diameter $D'(z)$ of the defocused image of a scattering volume in the diaphragm plane and the displacement $B'(z)$ of its center from the optical axis are as follows:

$$D'(z) = [\zeta D(z) + v D_r] f_r / z, \quad (5)$$

$$B'(z) = \zeta B(z) f_r / z. \quad (6)$$

The diameter $D'(z)$ decreases with the increasing z , and its center drifts towards the optical axis of the receiving objective (for a biaxial system) and approaches the focal plane. The trajectory of the displacement of this center is inclined to the optical axis of the receiving objective at an angle

$$\alpha = \arctan B(z) / f_r. \quad (7)$$

A part of the radiation flux from the point M that passes the diaphragm without a vignetting equals

$$d\Phi(r, \theta, z) = dP(r, \theta, z) K_t S_{M_{\text{eff}}}(z) / S'_M(z), \quad (8)$$

where $S_{M_{\text{eff}}}(z)$ is the area of intersection of the diaphragm aperture and the image spot within the circumferences of radii a and $d'_r/2$. By substituting Eqs. (1) and (4) into Eq. (8) and passing to the variables r', θ' in the diaphragm plane, we obtain total flux coming to the photodetector from the entire scattering volume sounded by integrating over the area of the image spot

$$\Phi(z) = \eta(z) P_0 T^2(z) K_t A_{\text{eff}} g(z) / z^2, \quad (9)$$

where

$$g(z) = 16\pi^{-2} [D'(z)]^{-4} \int_0^{D'(z)/2} r' dr' \times \int_0^{2\pi} S_{\text{eff}}(z) \kappa(r', \theta') d\theta', \quad (10)$$

and $S_{\text{eff}}(z)$ is the area of intersection of the diaphragm aperture and the spot of the scattering volume image (Fig. 3b).

The value $g(z)$, which enters into Eq. (9), characterizes the transmission coefficient of the receiving system. The coefficient is caused by vignetting of the backscattering radiation flux coming from the distance z and is called the lidar geometrical function (GF).^{3,5-9} It is defined by optical parameters of the lidar. Depending on the relation between them, different degrees of vignetting are possible^{3,8} (Fig. 3):

1) full vignetting in the blind zone (Fig. 3a, 3e), when $S_{\text{eff}}(z) = 0$, $g(z) = 0$;

2) the image spot only partially enters the diaphragm (see Fig. 3b) at

$$|a - D'(z)/2| \leq B'(z) \leq a + D'(z)/2, \quad (11)$$

$$S_{\text{eff}}(z) = a^2\{[2\arccos X_1 - \sin(2\arccos X_1)] + [D'(z)/2a]^2 [2\arccos X_2 - \sin(2\arccos X_2)]\}, \quad (12)$$

where

$$X_1 = \{[B'(z)]^2 - [D'(z)/2]^2 - a^2\} / 2aB'(z),$$

$$X_2 = \{[B'(z)]^2 + [D'(z)/2]^2 - a^2\} / 2aB'(z);$$

3) full transmission (Fig. 3c, 3d), $S_{\text{eff}}(z) = \pi[D'(z)/2]^2/4$ what corresponds to $g(z) = 1$ and takes place at $a > D'(z)/2$ and $B'(z) \leq a - D'(z)/2$.

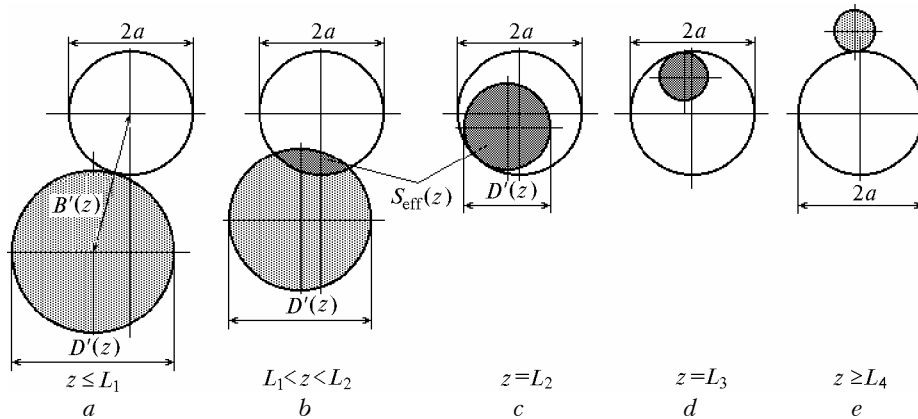


Fig. 3. Vignetting of the radiation flux coming from different distances z by the field stop diaphragm.

By substituting Eq. (12) into Eq. (10) and integrating, one can calculate GF of a particular lidar with the distribution $\kappa(r', \theta')$ over the cross section. Thus calculated results for uniform and Gaussian intensity distributions over the cross section of a laser beam can be found in Refs. 3, 5-7. Using the above considered technique, one can calculate GF of a lidar with SF having, for instance, a slit shape.¹⁵ A universal program for calculating lidar GF has been proposed in Ref. 22. Experimental methods for determining GF by use of movable screen-targets are also used (see, for instance, Refs. 23, 31).

4. Range limits of the geometric function

The calculated relations that are presented in this section generalize the results of Refs. 3, 8, which were obtained in a single scattering approximation.

Biaxial lidar. The boundary of the shadow zone $z = L_1$ (see Fig. 3a) is defined by the less root of the equation quadratic in z :

$$B'(z) = a + D'(z)/2, \quad (13)$$

$$L_1 = B_0 \frac{[(\xi + \gamma_{\parallel} \chi)^2 - \gamma_{\perp}^2 (1 - \chi^2)]^{1/2} - (\gamma_{\parallel} + \xi \chi)}{\xi^2 - (\gamma_{\parallel}^2 + \gamma_{\perp}^2)}, \quad (14)$$

where $\chi = (D_r + D_0)/2B_0$ is the packing coefficient; $\xi = a/\zeta f_r + \theta_0/2 - D_r z_0/2\zeta f_r^2$. If the optical axes are parallel ($\gamma_{\parallel} = \gamma_{\perp} = 0$) and $z_0 = 0$, we obtain

$$L_{10} = [2B_0 - (D_r + D_0)] / (2a/f_r + \theta_0). \quad (15)$$

The boundary $z = L_2$ (see Fig. 3c) is defined by the less root of the equation

$$B'(z) = a - D'(z)/2, \quad (16)$$

$$L_2 = B_0 \frac{[(\psi \chi - \gamma_{\parallel}) + (\psi + \gamma_{\parallel} \chi)^2 - \gamma_{\perp}^2 (1 - \chi^2)]^{1/2}}{\psi^2 - (\gamma_{\parallel}^2 + \gamma_{\perp}^2)}, \quad (17)$$

where $\psi = a/\zeta f_r - \theta_0/2 - D_r z_0/2\zeta f_r^2$. For $\gamma_{\parallel} = \gamma_{\perp} = 0$ and $z_0 = 0$, we obtain the well known expression

defining the distance, from which the lidar equation in a single scattering approximation becomes valid :

$$L_{20} = [2B_0 + D_r + D_0] / (2a / f_r - \theta_0). \quad (18)$$

Since the values $D_r, D_0, f_r,$ and θ_0 are usually set in calculating dimensions and energy potential of a lidar,²⁴ the boundaries L_1 and L_2 can be changed by changing the base B_0 and angle γ (mostly, by varying the diaphragm diameter $2a$ and the diaphragm displacement into the transfocal space of the objective). The displacement leads to a decrease in L_1 and L_2 .

As seen from Eq. (14), the condition $|\gamma| < \xi$ must be satisfied; otherwise, $L_1 \rightarrow \infty$ for $\gamma = \xi$. The formula (17) also imposes restrictions on the permissible value of the slope of optical axes, $|\gamma| < \psi$, so that the vignetting be stopped at a given distance. For $\gamma \geq \psi$, starting from the distance $z \geq L_3$, the vignetting can occur again, what is described by the second root of Eq. (16)

$$L_3 = B_0 \frac{[(\gamma_{\parallel} - \psi \chi) + [(\psi + \gamma_{\parallel} \chi)^2 - \gamma_{\perp}^2 (1 - \chi^2)]^{1/2}}{(\gamma_{\parallel}^2 + \gamma_{\perp}^2) - \psi^2}. \quad (19)$$

At the values $\gamma \geq \xi$ at $z = L_4$ (see Fig. 3e), full vignetting can occur; the second root of Eq. (13) is

$$L_4 = B_0 \frac{[(\gamma_{\parallel} + \xi \chi) + [(\xi - \gamma_{\parallel} \chi)^2 - \gamma_{\perp}^2 (1 - \chi^2)]^{1/2}}{(\gamma_{\parallel}^2 + \gamma_{\perp}^2) - \xi^2}. \quad (20)$$

As a rule, one chooses $\gamma < \psi$ and, in the range $L_2 \leq z < \infty$, the radiation flux is not vignetted. Figure 4 presents the relative value of the transition zone $L_2/L_1 = (1 + \chi)(1 + \mu) / (1 - \chi)(1 - \mu)$ which is obtained by dividing Eq. (18) by Eq. (15). Here $\mu = f_r \theta_0 / 2a$. Small values of the parameters χ and μ correspond to consideration of the intersection conditions for the optical axes of the receiving and transmitting systems in the object space.²⁵

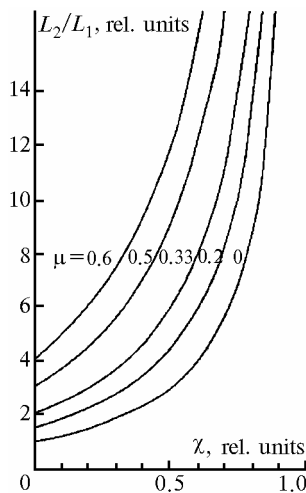


Fig. 4. The value of the lidar transition zone as a function of the relative parameters of the transmitter-receiver.

Figure 5 illustrates the influence of the angles γ_{\parallel} and γ_{\perp} upon the value L_2 ($L_{20} = L_2$ for $\gamma_{\parallel} = \gamma_{\perp} = 0$). Each value of the slope angle γ_{\parallel} in the plane YOZ corresponds to a critical value of the misalignment in the plane XOZ (see Fig. 2), $\gamma_{\perp cr} = (\psi^2 - \gamma_{\parallel}^2)^{1/2}$. When reaching the critical value, the interval of the operation zone $L_2 - L_3$ collapses to a point. This corresponds to the fact that the image spot emerges from the diaphragm just after entering it. Vertical lines in Fig. 5 correspond to this case.

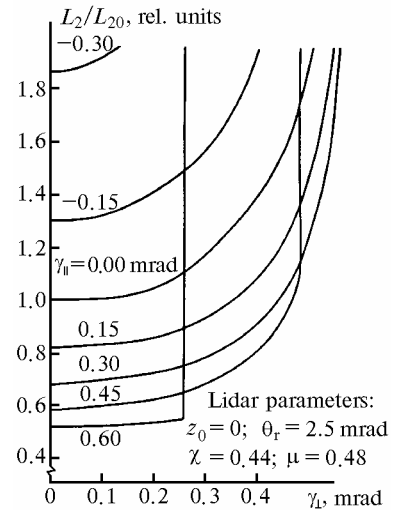


Fig. 5. Influence of optical axes misalignment upon the relative variation of the transition zone dimensions.

Coaxial lidar. For a coaxial system, $B_0 = 0$ and $B(z) = \gamma z$. The blind zone is formed due to shading of the central part of the objective by a screen of the diameter $2b \geq D_0$ (see Fig. 2a). In the range $0 \leq z \leq L_1$, the shading circle, which is defined by the radius $b'(z) = vb f_r / z$, exceeds the diaphragm diameter $2a$, and the radiation flux from the scattering volume does not reach the photodetector. The equation for determining the boundary of the blind zone ($z = L_1$) is

$$a + R'(z) = b'(z), \quad (21)$$

where $R'(z) = [D(z)/2 + B(z)] \zeta f_r / z$ is the boundary point on the diameter of a scattering volume image. By use of Eq. (21), we obtain

$$L_1 = (2b - D_0) / \{2[a + b(\zeta - 1)] / \zeta f_r + 2\gamma + \theta_0\}. \quad (22)$$

For $z_0 = 0$, the expression (22) can be reduced to: $L_{10} = (2b - D_0) / [2a / f_r + 2\gamma + \theta_0]$. From this it follows that the displacement of the diaphragm to the transfocal space leads to a decrease in L_1 .

The boundary of the transition zone, $z = L_2$, can be obtained from the equation (16):

$$L_2 = (D_r + D_0) / \{[2a + D_r(\zeta - 1)] / \zeta f_r - (2\gamma + \theta_0)\}. \quad (23)$$

If $z_0 = 0$, we obtain $L_{20} = (D_r + D_0) / [2a/f_r - (2\gamma + \theta_0)]$. As seen from Eq. (23), the condition $\gamma < \{[2a + D_r(\zeta - 1)] / \zeta f_r - \theta_0\} / 2$ must be satisfied; otherwise, $L_2 \rightarrow \infty$, and vignetting takes place over the whole interval of sounding range.

5. Requirements to the spatial filter and the efficiency criteria

Spatial filtration is a tool to separate out an optical signal from its mixture with the background noise. It is based on the distinctions in their spatial structure. For this purpose, a lidar SF must provide for their best separation. In most lidars, non-coherent spatial filtration is used, so the divergence θ_0 of the sounding radiation must be minimal to increase the density of its power and minimize dimensions of the scattering volume and the image $D'(z)$ corresponding to it. Within the frameworks of the theory of optimum linear filtration, two optimum criteria are most common: reaching either a minimum of the noise variance or a maximum of the signal-to-noise ratio at the SF output.^{26,27} The SFs applied in lidars use the second criterion.

We believe that the main efficiency criteria for SF are the following: 1) transmission coefficient and spatial boundaries of the interval of its action within the angular field of view or range; 2) the value of the signal-to-noise ratio. For a SF that is being used to controlled vignetting of a radiation flux, the error of the control law is an additional criterion.

From the viewpoint of SF application, lidar systems can be divided into two main groups: 1) those used for determining profiles of the atmospheric parameters (with the allowance for multiple scattering) and 2) for determining ranges to objects having high reflectivity contrast. For lidars from the first group, the information parameter of a signal is in its shape (amplitude or number of photo counts per time gate); so it is necessary to minimize the effect of the receiving system transmission and, correspondingly, of the SF on the shape of a lidar return within a given range. For lidars from the second group, accuracy in transmitting the shape of an echo signal is less significant. Proceeding from this, one differentiates the requirements to the SF.

The first of the efficiency criteria characterizes the information content of lidar systems. To increase it, the SFs of lidars from the first group must have transmission coefficient close to 1 in as wide range interval as possible. For lidars of the second group, the SFs must support a preset law of the radiation flux control with a minimal error also in a wide range interval. From the viewpoint of increasing the signal-to-noise ratio, requirements to SFs from both of these groups are similar.

As applied to lidars intended for sounding optically dense media, spatial filtration enables one to separate contributions coming from different orders of

multiple scattering to the received radiation flux that have different angular distribution within the field of view of the receiving system.^{12,13}

6. Matched and optimum diaphragms

In choosing diaphragm dimensions for lidars of the first group, two contradictory conditions must be satisfied. On the one hand, its aperture must be large enough to minimize the boundary L_2 to minimize vignetting and thus to increase the information content of sounding. On the other hand, the aperture must be decreased to reduce the background radiation flux. As shown in Sec. 3, on a biaxial lidar, the spot of the scattering volume image moves along a trace in the diaphragm plane with increasing z . The boundaries of the trace define the minimum size of a region necessary to transmit the radiation flux without vignetting. So the dimensions of a round aperture can be decreased⁴ to decrease the background flux. The diaphragm whose shape coincides with the track of the moving image spot is considered to be *matched*.

Assigning the initial L_2 and maximal L_m sounding ranges, we obtain by Eq. (5) the radius of the large $r_1 = D'(L_2)/2$ and small $r_2 = D'(L_m)/2$ arcs restricting the diaphragm along the axis of symmetry. The distance between their centers is $d = \zeta f_r [B'(L_2)/L_2 - B'(L_m)/L_m]$; their positions can be obtained from Eq. (6). Here L_2 is defined by the energy potential of the lidar.²⁸ The matched diaphragm (Fig. 6) is mounted so that the center O coincides with the image center at $z = L_m$, and the axis OY lies in the same plane as the optical axes of the receiving and transmitting systems. For a comparison, Fig. 6 presents a usual diaphragm centered on the optical axis of the receiver to provide the same value L_2 . In mounting the matched diaphragm into the focal plane ($L_m \rightarrow \infty$), the formulas for the dimensions become simpler: $r_1 = f_r [(D_r + D_0) / L_2 + \theta_0] / 2$, $r_2 = f_r \theta_0 / 2$, $d = f_r B_0 / L_2$.

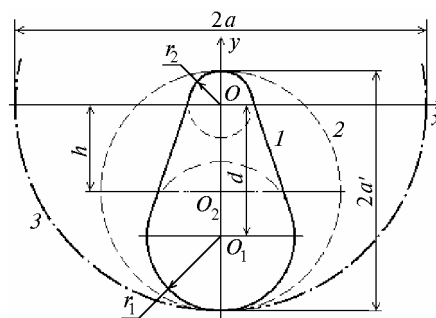


Fig. 6. Diaphragms of reduced dimensions: matched (1); round off-center (2); usual centered (3).

One can additionally decrease the cross size of the matched diaphragm and make it *optimal* by mounting it in the transfocal space of the receiving objective, according to Eq. (7), at an angle α to its optical axis.

Then the cross size of each part of the diaphragm along the axis OX is more accurately conjugated with the diameter of the scattered volume image and has the minimum value

$$D'_{\min}(z) = D(z) f_r / z \quad (24)$$

(see Eqs. (24) and (5) for a comparison). Because of the inclined position of an optimum diaphragm, the arcs of radii r_1 and r_2 are transformed into parts of ellipses with the major axes $D'_{\min}(L_2)/\sin\alpha$ and $D'_{\min}(L_m)/\sin\alpha$ and minor axes $D'_{\min}(L_2)$ and $D'_{\min}(L_m)$. The distance between the centers of the ellipses is $d' = d/\sin\alpha$. The area of the projection of the optimum diaphragm onto the focal plane is smaller as compared with the matched one. The optimum diaphragm provides for the best signal-to-noise ratio at non-vignetted reception of the backscattered radiation from the entire path $L_2 - L_m$ due to minimal cross size. Use of diaphragms of the matched and optimum shapes enables one to enhance the information content of lidar sensing with such systems due to shorter range L_2 and increased upper boundary of a lidar return signal.⁴

Instead of a diaphragm of the matched shape, one can use a round one⁴ with the diameter

$$2a' = r_1 + r_2 + d. \quad (25)$$

If it is installed in the focal plane, we have

$$2a' = f_r [B_0 (\chi + 1) / L_2 + \theta_0]. \quad (26)$$

The center of the diaphragm is displaced with respect to the axis OY (see Fig. 6) by the value $h = (d + r_1 - r_2) / 2$. Because of a smaller size the off-center round diaphragm enables one to increase the signal-to-background ratio by a factor of $4 / (1 + \varepsilon)^2$ as compared with a centered diaphragm of the diameter $2a$ providing for the same value L_2 . Here $\varepsilon = \theta_0 L_2 / (2B_0 + D_r + D_0 + \theta_0 L_2)$. At $\varepsilon \leq 0.1$ one can obtain almost 4-fold reduction of the background level. For the matched diaphragm, the increase of the signal-to-background ratio is even higher.

In a realistic lidar, inaccuracy of the alignments, deformation of optical systems, and possible aberrations lead to additional broadening of the image spot in the diaphragm plane what requires an increased size of the diaphragm. Finally, the influence of these factors can be taken into account in calculation formulas by equivalent increase of the divergence angle θ_0 of the sounding beam.

The influence of the objective's aberrations which increase as the image points move away from the optical axis can be reduced by choosing the corresponding value of the angle γ_{\parallel} .⁴ According to Eqs. (2) and (6), $B'(z)$ depends on $h = a' - f_r(\theta_0/2 + \gamma_{\parallel})$ and the displacement of the center of the considered diaphragm is $h = 0$. It can be centered on the optical axis by putting $h = 0$ what can be reached at $\gamma_{\parallel \text{opt}} = a' / f_r - \theta_0 / 2$. In this case, the images of the scattering volumes from the entire sounding path from L_2 to $L_m \rightarrow \infty$ are closer

to the optical axis of the objective. This weakens the influence of aberrations and makes the diameter of an actually needed diaphragm closer to the size defined by relations (25) or (26). In the same way, one can arrange the matched and optimum diaphragms.

In coaxial lidars ($B_0 = 0$) with coinciding ($\gamma = 0$) or diverging ($\gamma \neq 0$) axes of the receiving and transmitting systems, the image of a scattering volume remains centered about either the optical axis of the objective at $\gamma = 0$ or a straight line parallel to this axis and shifted from it by the distance $h = \gamma f_r$. The diaphragm is centered with respect to this straight line and its aperture must correspond to the shape of the sounding beam cross section. The dimensions of the diaphragm are to be chosen with the account of the boundaries of the blind and transition zones L_1 and L_2 .

7. Controlling diaphragms and rasters

Using the results presented in previous sections, we analyze SF intended for controlled vignetting of the backscattered radiation flux.

The profile of a diaphragm *compensating for z^{-2} dependence* in the lidar return signal has been analyzed by the authors together with S.A. Danichkin for a biaxial lidar in the case when the diaphragm is installed (see Fig. 1e) in the focal plane of the objective under the condition that illumination is distributed uniformly over the image spot of the diameter $D'(z)$ and $\gamma = \gamma_{\parallel}$, while $\gamma_{\perp} = 0$. In the transition zone, $L_1 < z < L_2 = z_b$, this spot moves and fills the lower part of the diaphragm. This part is formed by a semicircle of r_0 radius while the leading edge of a return signal is formed. Controlled vignetting begins at $z \geq z_b$ when the diaphragm transmits a portion of the radiation flux defined by Eq. (12) for $a = r_0$, $B'(z_b) = y_b$ and $D'(z_b) = 2\rho(z_b)$:

$$S_{\text{eff}}(z_b) = \pi r_0^2 / 2 + r_0 [\rho^2(z_b) - r_0^2]^{1/2} + \rho^2(z_b) \arcsin[r_0 / \rho(z_b)] - 2r_0(y_b - h), \quad (27)$$

where h is the distance between the center of the arc of radius r_0 and optical axis of the objective. The boundaries L_1 and L_2 are determined from the conditions $B'(L_1) = h + r_0 + \rho(L_1)$ and $B'(z_b) = h + [\rho^2(z_b) - r_0^2]^{1/2}$. The condition for the z^{-2} compensation to work is $\frac{d}{dz} \frac{S_{\text{eff}}(z)}{z^2 \pi \rho^2(z)} = 0$ that is satisfied at

$$S_{\text{eff}}(z) = C z^2 \pi \rho^2(z), \quad (28)$$

where the value C is to be determined. Now we suppose that $\rho(z) = \rho_0 [1 + (D_r + D_0) / \theta_0 z]$, and $\rho_0 = f_r \theta_0 / 2$ is the spot radius at the distance z_e (by the end of the control zone). The former is valid for $(D_r + D_0) / \theta_0 z_e \ll 1$. For weakly collimated beams, one can take $\rho(z) = \rho_0$ within the entire interval $z_b \leq z \leq z_e$ under condition that

$$(D_r + D_0)/\theta_0 z_b \ll 1. \quad (29)$$

One can see from Fig. 1e that, for $z > z_b$, the area $S_{\text{eff}}(z)$ is formed by the upper arc segment which is described in the diaphragm coordinates by the expression $y_{\text{up}} = [\rho^2(z) - x^2]^{1/2} - y_1$, where $y_1 = B'(z)$. Its lower part is determined by a semicircle of radius r_0 . The lateral sides are defined by the diaphragm profile $y_{\text{lat}}(x)$, the expression for which is to be obtained. The function $y_{\text{lat}}(x)$ must satisfy three conditions: $y_{\text{lat}}(r_0) = -h$; $y_{\text{lat}}(\rho_0) = f_r (B_0/z_e - \gamma_{\parallel})$; $dy_{\text{lat}}(x)/dx = 0$. For the interval $z_b \leq z \leq z_e$, we have

$$S_{\text{eff}}(z) = \pi r_0^2/2 + X[\rho^2(z) - X^2]^{1/2} + \rho^2(z) \times \\ \times \arcsin[X/\rho(z)] + 2(r_0 h - X y_1) - 2 \int_{r_0}^X y_{\text{lat}}(x) dx, \quad (30)$$

where the value $x = X$ is defined so that the curves intersect: $y_{\text{up}}(X) = y_{\text{lat}}(X)$. By differentiating Eq. (30) with respect to z , we obtain

$$dS_{\text{eff}}(z)/dz = 2f_r B_0 \{X - \chi \rho(z) \arcsin[X/\rho(z)]\} / z^2, \quad (31)$$

where, as above, $\chi = (D_r + D_0)/2B_0$. Under condition (29) the expression (31) reduces to a simpler form:

$$dS_{\text{eff}}(z)/dz = 2f_r B_0 X / z^2. \quad (31=)$$

Differentiating Eq. (30) with respect to z and equating it to Eq. (31), we have

$$2Cz \pi \rho(z) \rho_0 = 2f_r B_0 \{X - \chi \rho(z) \arcsin[X/\rho(z)]\} / z^2, \quad (32)$$

by use of which, and two boundary conditions

$$X = r_0 \text{ at } z = z_b \text{ and } X = \rho_0 \text{ at } z = z_e, \quad (33)$$

we obtain the expression relating the initial and final distances:

$$z_e/z_b = \sqrt[3]{(1 - \chi\pi/2) / \{r_0/\rho(z_b) - \chi \arcsin[r_0/\rho(z_b)]\}}. \quad (34)$$

Since the ratio $r_0/\rho(z_b) \ll 1$ always holds, $z_e/z_b = k_{\text{lat}} \times \{\rho_0[1 + (D_r + D_0)/\theta_0 z_b]/r_0\}^{1/3}$, where the coefficient $k_{\text{lat}} = [(1 - \chi\pi/2)/(1 - \chi)]^{1/3}$ imposes restrictions on the minimum value of the spacing between the axes, $B_{0\text{min}} = \pi(D_r + D_0)/4$. The coefficient k_{lat} rapidly decreases as χ tends to $\chi_{\text{max}} = 2/\pi$. This makes the interval, where z^{-2} is compensated for, shorter. It is worth choosing $B_0 > (D_r + D_0)$. Under the condition (29), the expression (34) reduces to

$$z_e/z_b = (\rho_0/r_0)^{1/3}. \quad (34=)$$

Determining the value C by use of Eq. (33), we obtain, by making use of Eq. (32), the equation for coordinates of the lateral diaphragm contour. The equation relates X to z :

$$X/\rho(z) - \chi \arcsin[X/\rho(z)] = \{r_0/\rho(z_b) - \\ - \chi \arcsin[r_0/\rho(z_b)]\} z^2 \rho(z) / z_b^3. \quad (35)$$

It is a transcendental equation relative X and can be solved only numerically if lidar parameters and the quantities r_0 , ρ_0 , and h are known. If inequality (29) holds, $X = r_0(z/z_b)^3 = \rho_0(z_e/z)^3$. Then, from the condition $y_{\text{up}}(X) = y_{\text{lat}}(X)$ we obtain the expression for the profile of the lateral side of the diaphragm compensating for z^{-2} :

$$y_{\text{lat}}(x) = [\rho_0^2 - x^2]^{1/2} - f_r B_0 [(\rho_0/x)^{1/3} / z_e - \gamma_{\parallel} / B_0]. \quad (36)$$

One can see from Eq. (34a) that, to broaden the interval of control at a given value ρ_0 , it is necessary to minimize r_0 . At the same time, since $S_{\text{eff}}(z_b) \approx \pi r_0^2/2$, the radius r_0 defines the minimum level of power Φ_0 transmitted through the diaphragm when regulating the radiation flux. It is easy to demonstrate that $r_0 = \rho_0 [2\Phi_0/P(z_b)]^{1/2}$, where $P(z_b)$ is the flux of radiation entering the diaphragm in the beginning of the process of controlled vignetting. Taking into account Eq. (34a), we have $z_e/z_b = [P(z_b)/2\Phi_0]^{1/6}$. The value Φ_0 is defined by the necessary excess of a lidar return over noise. Assuming the attenuation $P(z_b)/\Phi_0 = 2 \cdot 10^6$, we obtain that compensation in this case is achievable in the range multiple to 10. Thus, the compression coefficient for the dynamic range of a lidar signal²⁹ G achievable is 100. With the increase in Φ_0 , the range interval of the efficient control, $z_b - z_e$, becomes narrower. Analysis of the diaphragm contour presented here is more accurate as compared with that in Ref. 18. The latter was performed considering intersection of the cones of directional patterns of the transmitting and receiving systems in the space of objects. The diaphragm compensating for z^{-2} considerably decreases the level of background radiation fluxes due to its reduced area. However, starting from the distance $z \geq z_e$, it is impossible to compensate for the decrease in the received power by an increase in the diaphragm size because its dimension along the x axis reaches the maximum equal to the radius of the image spot ρ_0 . Continued vignetting of the radiation flux at the range $z \geq z_e$ leads to its quick decrease and reduces the energy potential of the lidar (Fig. 7).

To eliminate this shortcoming, a special controlling diaphragm was proposed.³⁰ It introduces maximal vignetting of the lidar return from near distances when their intensity is high; besides, it increases transmitting with increasing z so that the optical flux passes through the diaphragm completely at the maximum distance z_f . In this case, its contour (Fig. 8) is formed by a combination of an arc of a circle with radius $\rho_0 = f_r \theta_0/2$. The arc is tangent to the lateral sides of the diaphragm which are formed by the second order curves. These curves, in their turn, are tangent to each other and to the axis of symmetry of the diaphragm; the point of tangency of the curves, which describe the lateral sides, is spaced from the circle center by the distance $h = f_r B_0(1/z_b - 1/z_e) - \rho(z_b)$. If z_f does not tend to infinity, the center of

the circle of radius r_0 must be displaced from the axis of the receiving objective by a distance equal to $f_r B_0/z_e$. Reducing the dynamic range of the radiation flux, the diaphragm does not limit the energy potential of the lidar (see Fig. 7). As shown in Ref. 2, the highest degree of vignetting can be achieved with a diaphragm having its lateral sides formed by a circle arc with the radius $R = (h^2 - \rho_0^2)/2r$.

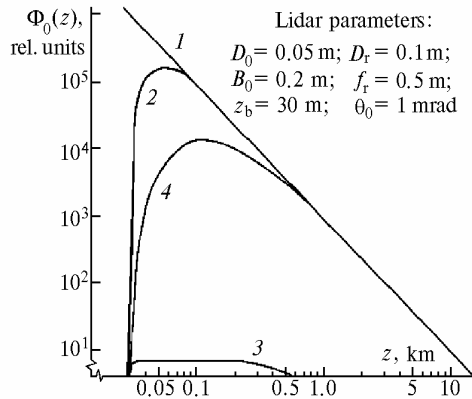


Fig. 7. Radiation flux passing through different SF: non-vignetted reception (1); usual centered diaphragm (2); diaphragm compensating for z^{-2} (3); controlling diaphragm (4).

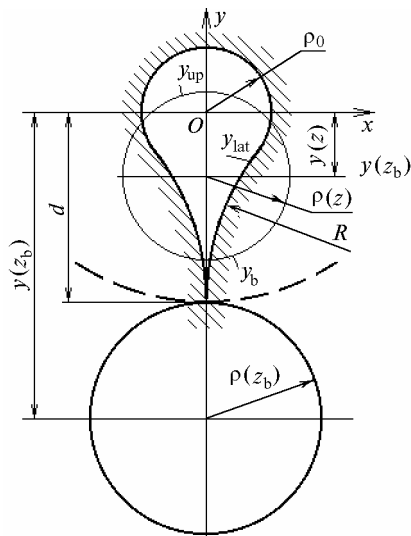


Fig. 8. The profile of a vignetting diaphragm.

A film raster in the form of an optical wedge¹⁶ when applied to compensate z^{-2} , can be placed in the focal plane of an objective, provides for variation of the transmission factor no more than by 200 times. This is caused by the maximum possible density of photographic materials. Since the image spot has a finite diameter $D'(z)$, the radiation flux arrived from the distance z passes simultaneously through the wedge parts having different transmission coefficients. So it is impossible to obtain exact compensation for the z^{-2} dependence of the lidar return. Technologically fabrication of a small-size optical wedge is difficult. To overcome this difficulty, it was proposed in Ref. 16, to increase the trajectory of

the image spot, and the base B_0 equal to 3 m was used to achieve this task. The value f_r was chosen to be small to reduce the diameter $D'(z_b)$.

Like the diaphragm of optimum shape, the raster compensating for z^{-2} dependence of the received radiation flux ought to be mounted in the transfocal space of the objective so that the normal to its surface and the axis of symmetry be in the plane passing through the optical axes of the receiving and transmitting systems¹⁷ and its axis of symmetry being inclined relative to the axis of the receiving objective at an angle α defined by the relation (7). In this case, the image has the minimal diameter (24) at each point of the axis of the filter-raster. Figure 9 presents the optical arrangement of a lidar, in which SF is a plane mirror with the reflection factor $R_{min} \leq R(z) \leq R_{max}$ variable along the axis of symmetry $O_1O'_1$.¹⁷ The radiation flux, scattered in the medium at the distance z_b and passing through a usual diaphragm without vignetting, falls onto the mirror part with $R(z) = R_{min}$ which is most distant from the diaphragm. With the increase in z , intensity of incident radiation decreases and the image spot is displaced over the mirror along the axis $O_1O'_1$ into the domain with the increasing value of $R(z)$. The position of the mirror part with the required value of $R(z)$ on its surface is defined by the expression $y = B_0 f_r [R_{max}/R(z)]^{1/2}/z_e$ where y is the distance along the axis $O_1O'_1$ from the point of its intersection with the focal plane of the objective. The images of scattering volumes, according to Eq. (24), will be minimal because they are in the mirror plane independently of distance. If the condition (29) is fulfilled, $D'_{min}(z) = f_r \theta_0$ and the mirror parts with different reflection factors will overlap within the image to a lesser degree. Therefore, the law of z^{-2} compensation should fulfill more accurately as compared with the case when the controlling SF is mounted in the focal plane. The maximum value of the compression coefficient of the dynamic range G achievable with such an SF is less than 96.

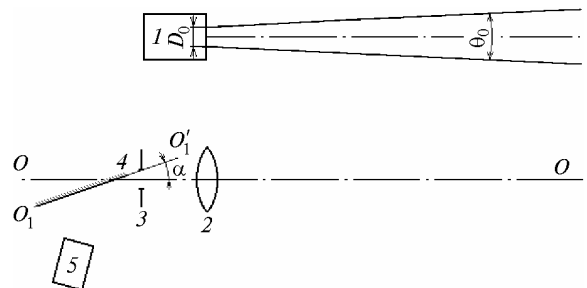


Fig. 9. Mirror-based compensating SF: transmitting system (1); receiving objective (2); diaphragm (3); mirror (4); photodetector (5).

Comparative characteristics of the controlling SFs with respect to the transmission coefficient are presented in Fig. 7. It should be noted that misalignment between the optical axes of the receiving and transmitting systems and redistribution of radiation

intensity over the spot of the scattering volume image, what is caused by atmospheric turbulence or by the source itself, lead to violation of z^{-2} law compensation. So it is helpful to use controlling SFs in lidars of the second group. Besides, to finally form the field of view of a lidar receiving system, a raster SF (mirrors and optical wedges) require additional diaphragms to suppress the background flux either in the focal plane of the objective or by combining it with the optimum diaphragm and a raster.

8. Diaphragms and rasters for analysis of multiple scattering and special SF

In sounding optically dense media (clouds, smoke plumes), effects of multiple scattering (MS) lead to an increase in the scattering volume size as the laser pulse enters the cloud.^{13,31} In this case, single scattered radiation with a certain portion of MS comes from a volume spanned by the diameter $D(z) = D_0 + \theta_0 z$. Beyond this diameter, doubly and multiply scattered radiation is formed. In sounding distant clouds, the condition (29) is fulfilled; so, in the objective's focal plane, the diameter which is defined by formula (5) is $D'(z) \approx 2\rho_0 = f_r \theta_0$. Using a receiving system with several fields of view characterized by $\theta_r > \theta_0$, one performs spatial selection of multiple scattering orders when viewing different parts of the scattering volume.^{12,31-34}

In studying the MS effects, to simplify the SF constructions, it is worth using coaxial lidars in which the image spot does not move in the filter plane. Here the SF are made as circle and ring diaphragms of different diameter, which are centered about the optical axis of the objective ($\gamma = 0$). Shading of the central part of the diaphragm by a circle $2\rho_0$ (see Figs. 1a and 1c) enables one to isolate only the MS radiation that enters the photodetector.³² All the SF can be divided into two groups: 1) SF that enable one to measure the flux of MS radiation in different fields of view simultaneously and 2) sequential SF (accessory diaphragms), in which the change of the field of view must occur during time less than temporal fluctuations of the medium. The required range for variation of the field of view is $\theta_r = 0.1 - 10$ mrad.^{12,32}

Different types of SF with several fields view applied to studies of the MS effects are considered in Ref. 12. One of them is a device based on a matrix of four concentric photodiodes with the diameters 0.75, 2.5, 5.0, and 7.6 mm. The device is placed in the focal plane of the objective. The transmission function of such a SF is similar to that presented in Fig. 1c with different distribution of the parts with $\overline{f(x, y)} = 1$. It makes it possible to measure MS radiation received within different fields of view simultaneously. The second similar type of the SF is a ring-shaped holographic element placed in the image plane and that uses the first-order diffraction of incident light at

different angles to direct it to different photodetectors. Its main drawback is low coefficient of incident wave transformation into the first-order diffraction (no more than 30%). The third type of SF refers to sequential ones and is a set of accessory mesomorphic round masks with the diameters from 18.7 μm to 6.11 mm. The transmission coefficient of the masks is 42% in their open state and attenuation 10^{-5} in the closed state. Transmission is controlled by a computer. Spatial filters of the fourth type usual need some accessory diaphragms of the diameter from 76 to 9424 μm (32 round apertures). The apertures are at the periphery of a revolving disc and provide for variation of the field of view angle in the range from 0.1 to 12.4 mrad, while the variation step of the diameter is $\sim 17\%$.

In Ref. 13, a movable end of an optical wave guide, by use of which a part of the received flux was sent to the photodetector, was used as a SF to study MS radiation flux which is formed in the focal plane of the objective around the image of a sounding beam of diameter $2\rho_0$. The flat end of a monofiber with the diameter $2a_f$ plays the part of a diaphragm but the limiting incidence angle for the beam entering the fiber end is $u = \arcsin \sqrt{n_f^2 - n_o^2}$. This angle is $10 - 20^\circ$ depending on the relation between n_f and n_o and the length of the fiber.³⁵ The latter must be taken into account in matching the SF with the objective's parameters. It is also possible to create a multifiber bundle so that individual groups of fibers form concentric circles of different diameters at the one end of the bundle while at the other end being collected into bunches directing radiation from these rings to individual photodetectors. Having $f(x, y)$ similar to the matrix of concentric photodiodes, such a SF makes it possible to measure MS radiation received within different fields of view simultaneously.

Measurements of the wind velocity with lidars by the correlation technique³⁶ require the sensing of the atmosphere to be performed along several directions different to each other by $\sim 6-7^\circ$. For this purpose, we have designed a wide-angle objective based on the Schmidt camera with a special SF. The latter is a disc with several small diaphragms with the diameter $2a_m$ mounted in the focal plane of the objective (Fig. 10).

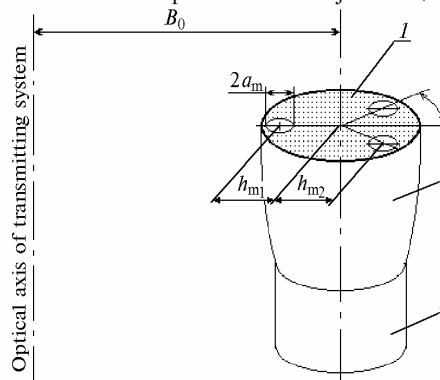


Fig. 10. Matrix SF: matrix diaphragm (1); focone (2); photodetector (3).

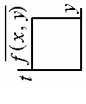
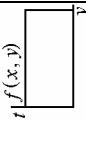
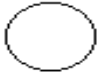
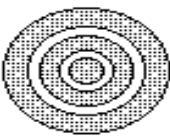
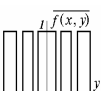
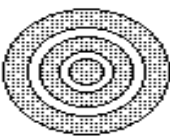
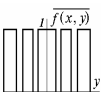
The centers of the diaphragms are shifted with respect to the optical axis at the distances h_{m1} ($h_{m2} = h_{m1} \cos\beta$, where β is the angle between the plane containing the optical axes of the receiving and transmitting systems and the direction from the disc center toward the corresponding diaphragm). This SF enables one to realize narrow fields of view, $\theta_{r,m} = 2a_m/f_r$, for different directions $\gamma_m = h_m/f_r$ with respect to the optical axis of the receiving system. When the values of angle γ_m are about a few grades, the diameter $2h_{m1}$ exceeds the entrance aperture of the photodetector. So, to collect the received radiation fluxes onto one photodetector, we applied a focone made from K-8 glass and mounted it behind the diaphragm. The diameters of the input and output ends of the focone are

52 and 22 mm, respectively; its side surface is formed by an arc of radius 422 mm. This SF provided, at small instant angle $\theta_{r,m} = 6$ mrad, for receiving scattered radiation arriving from the directions separated by $\sim 6^\circ$ with a stationary receiving system, oriented along a fixed direction.

9. Comparative analysis of the spatial filters of a lidar

The above considered SFs can be divided into three large groups: diaphragms, optical wave guides, and rasters. The SF classification proposed, including the SF shapes, corresponding transmission functions $f(x, y)$, and characteristic parameters are presented in the Table 1.

Table 1. Characteristics of the lidar SFs

Filter type	Shape	$f(x, y)$	Parameters	Note
Diaphragm	round 		<i>centered</i> diameter $2a$, displacement from the focal plane $0 - +z_0$ <i>off-center</i> diameter $2a'$, displacement from the axis h	
	matched 		the SF shape is defined by the shape of the image spot "trace" in the diaphragm plane	
	optimum 		same as above	inclined to the focal plane at the angle $\alpha = \arctan f_r/b_0$
	controlling 		the range interval of control $z_e/z_b \leq 10$	
Light guide	monofiber 	< 1	defined by the optical wave guide parameters	the limiting aperture angle $u = \arcsin \sqrt{n_f^2 - n_o^2}$
	multifiber bundle 		idem	fibers of concentric rings are united in individual bunches
Raster	optical wedge transmission 		maximum attenuation ~ 200 $z_e/z_b \leq 14$	
	mirror reflection 		$z_e/z_b \leq 10$	inclined to the focal plane at the angle $\alpha = \arctan f_r/b_0$
	ring concentric photodetector 		photosensitive surface defines the raster shape	

10. Conclusion

Analysis of different SFs performed, which form the field of view of a lidar receiving system, is based on constructing the image of a scattering volume in the SF plane and determining the transmission function of the filter. This allows one to consider from the general stand point all the operation features of SF for different purposes. A list of main characteristics and efficiency criteria for SF is considered. The shape of matched and optimum diaphragms that increase the signal-to-background ratio achieved with the biaxial lidars is determined. Comparison of diaphragms and rasters intended for controlled vignetting of the received radiation flux in a given range interval is performed. Different SFs of lidars for measuring multiple scattering and determining wind velocity by the correlation technique are considered.

References

1. A.I. Abramochkin and A.A. Tikhomirov, *Atmos. Oceanic Opt.* **11**, No. 8, 768–780 (1998).
2. A.A. Tikhomirov, in: *Measurement of the Atmosphere Optical and Meteorological Parameters Using Laser Radiation* (Publishing House of the Institute of Atmospheric Optics S" AS SSSR, Tomsk, 1980), pp. 106–113.
3. A.A. Tikhomirov, in: *Abstracts of Reports at Fourth All-Union Symposium on Laser Sounding of the Atmosphere* (Publishing House of the Institute of Atmospheric Optics S" AS SSSR, Tomsk, 1976), pp. 301–304.
4. A.I. Abramochkin, S.A. Danichkin, and A.A. Tikhomirov, in: *Abstracts of Reports at the Fifth All-Union Symposium on Laser Sensing*, Institute of Atmospheric Optics S" AS SSSR, Tomsk (1978), Part II, pp. 60–62.
5. T. Holldorson and J. Langerholc, *Appl. Opt.* **17**, No. 2, 240–244 (1978).
6. J. Harms, W. Lahmann, and C. Weitkamp, *Appl. Opt.* **17**, No. 7, 1131–1135 (1978).
7. J. Harms, *Appl. Opt.* **18**, No. 10, 1559–1566 (1979).
8. S.A. Danichkin and I.V. Samokhvalov, *Opt. Mekh. Promst.*, No. 5, 5–8 (1979).
9. S.A. Danichkin, T.M. Kuchevskaya, and A.A. Tikhomirov, in: *Abstracts of Reports at the Seventh All-Union Symposium on Laser Sensing*, Institute of Atmospheric Optics S" AS SSSR, Tomsk (1982), Part II, pp. 204–207.
10. A.I. Abramochkin and A.A. Tikhomirov, in: *Instrumentation and Methods for Remote Sounding of the Atmosphere* (Nauka, Novosibirsk, 1980), pp. 19–29.
11. A.I. Carswell and S.R. Pal, *Appl. Opt.* **19**, No. 24, 4123–4126 (1980).
12. G. Roy, L. "issonnette, and Cr. "astille, in: *Abstracts of Reports at 19th Intern. Laser Radar Conf.* (1998), Part 2, pp. 767–770.
13. C. Werner, J. Streicher, H. Herrmann, and H. Dahn, *Opt. Eng.* **31**, No. 8, 1731–1745 (1992).
14. Yu.F. Arshinov, S.M. "obrovnikov, N.". Serikov et al., *Atmos. Oceanic Opt.* **10**, No. 3, 221–224 (1997).
15. Yu.F. Arshinov, S.M. "obrovnikov, S.A. Danichkin, et al., *Problems of Remote Sensing of the Atmosphere* (Publishing House of the Institute of Atmospheric Optics S" AS SSSR, Tomsk, 1975), pp. 150–153.
16. V.S. Gorshkov, V.I. Eremin, K.S. Lamden, et al., in: *Abstracts of Reports at Fourth All-Union Symposium on Laser Sounding of the Atmosphere*, (Publishing House of the Institute of Atmospheric Optics S" AS SSSR, Tomsk, 1976), pp. 101–102.
17. S.A. Danichkin, V.N. Marichev, and A.A. Tikhomirov, *Inventor's Certificate No. 1065743*, "ull. Izobret., No. 1 (1984).
18. "I. Metlitskii and E.A. Chayanova, *Trudy Central Astrophys. Obs.* No. 130, 81–89 (1977).
19. C.A. Northend, R.C. Honey, and W.E. Evans, *Rev. Sci. Instr.* **37**, No. 4, 393–400 (1966).
20. M.I. Apenko and A.S. Dubovik, *Applied Optics* (Nauka, Moscow, 1971), 392 pp.
21. GOST 7427–76. *Geometrical Optics. Terms, Definitions, and Literal Designations* (Gosstandart, Moscow, 1984).
22. I.A. Razenkov, Yu.M. Andreev, and N.A. Shefer, *Atmos. Oceanic Opt.* **9**, No. 10, 905–908 (1996).
23. Y. Sasano et al., *Appl. Opt.* **18**, No. 23, 3908–3910 (1979).
24. A.I. Abramochkin and A.A. Tikhomirov, in: *Problems of Remote Sensing of the Atmosphere* (Publishing House of the Institute of Atmospheric Optics S" AS SSSR, Tomsk, 1976), pp. 21–32.
25. A.L. Skrelin, A.P. Ivanov, and I.I. Kalinin, *Izv. Akad. Nauk SSSR, Ser. Fiz. Atmos. Okeana* **6**, No. 9, 889–899 (1970).
26. V.P. Savinykh and V.A. Salomatin, *Optical Electronic Systems of Distant Sounding* (Nedra, Moscow, 1995), 315 pp.
27. H. Stark, ed., *Application of Optical Fourier Transforms* (New York, Academic Press, 1982).
28. "V. Kaul', *Atm. Opt.* **2**, No. 2, 166–169 (1989).
29. A.A. Tikhomirov, in: *Abstracts of Reports at Seventh All-Union Symposium on Laser and Acoustic Sounding*, Institute of Atmospheric Optics S" AS SSSR, Tomsk (1982), pp. 169–172.
30. S.A. Danichkin, and A.A. Tikhomirov, *Inventor Certificate No. 676962*, "ull. Izobret., No. 28 (1979).
31. M.V. Kabanov, ed., *Laser Sensing of Industrial Aerosols* (Nauka, Novosibirsk, 1986), 186 pp.
32. R.J. Allen and C.M.R. Platt, *Appl. Opt.* **16**, No. 12, 3193–3199 (1977).
33. A.I. Abramochkin, V.V. Zanin, I.E. Penner, et al., *Atm. Opt.* **1**, No. 2, 92–96 (1988).
34. S.R. Pal and A.I. Carswell, *Appl. Opt.* **24**, No. 12, 3464–3471 (1985).
35. N.S. Kapany, *Fiber Optics. Principles and Application* (New York, Academic Press, 1967).
36. G.G. Matvienko, Yu.F. Arshinov, A.I. Grishin, et al., in: *Proceedings of the 11th Symposium on Laser and Acoustic Sounding of the Atmosphere* (Publishing House of Institute of Atmospheric Optics S" RAS, Tomsk, 1993), pp. 130–136.